Quality Assurance for the Manufacturing of Oxide Fiber Reinforced Ceramic Composites for Aerospace Applications

Thomas ULLMANN[*], Yuan SHI[*], Nils RAHNER[**], Martin SCHMÜCKER[**]
Peter FEY[***], Gerhard BUSSE[***] and Stefan BECKER[****]

[*] German Aerospace Center, Pfaffenwaldring 38-40, 70569 Stuttgart, Germany
[**] German Aerospace Center, Linder Höhe, 51147 Cologne, Germany
[***] Institute of Polymer Technology IKT, Univ. of Stuttgart, Pfaffenwaldring 32, 70569 Stuttgart, Germany
[****] Becker Photonik GmbH, Portastr. 73, 32457 Porta Westfalica, Germany

Abstract. The processing route of a CMC material comprises several very complex manufacturing procedures which have to be optimized down to the last detail and, if necessary, monitored and controlled continuously. Consequently, non-destructive inspection techniques are important tools to provide the necessary information that is needed to understand the microstructure and to identify the failure-relevant defects that may occur during manufacturing. The examples discussed here are focusing the manufacturing and material properties of the wound highly porous oxide ceramic matrix composite (WHIPOX™) developed by DLR. It is reported about inspection results with air-coupled ultrasound, optically excited lock-in thermography, 3D terahertz imaging and computed tomography (µ-CT, nano-CT). Furthermore, mechanical properties of WHIPOX samples which are obtained from tensile and Iosipescu shear tests are correlated with non-destructive inspection results from lock-in thermography and high resolution CT analysis.

Introduction

Oxide fiber reinforced oxide ceramic matrix composites, so called oxide CMCs, are promising materials for high temperature applications under harsh environmental conditions. Unlike monolithic ceramics CMC materials are damage tolerant and thermal shock resistant. The wound highly porous oxide ceramic matrix composite (WHIPOX™) is a special type of oxide CMC material that was developed by the Institute of Materials Research of the German Aerospace Center in Cologne. Due to its excellent thermo-mechanical properties WHIPOX CMCs show high potential for structure components of thermal protection systems (TPS) and for many other high temperature applications as for example combustion chamber shingles, fuel injection heads or firing nozzles [1]. Beside this the transparency for radio signals was another important reason for selecting this material for the SHEFEX I and II reentry vehicles [2]. Thus, the WHIPOX segments that were used on these flying missions accomplished both tasks as thermal protection components as well as a transmission window for the data telemetry system. The attached panels of the naturally white material appear black because of an additional environmental barrier surface coating which ensures adequate corrosion resistance and improves thermal heat emission (Fig. 1). The uncoated CMC material is depicted in Figure 2. WHIPOX was also used as a seal between the other carbon fiber based CMC panels of SHEFEX [2].

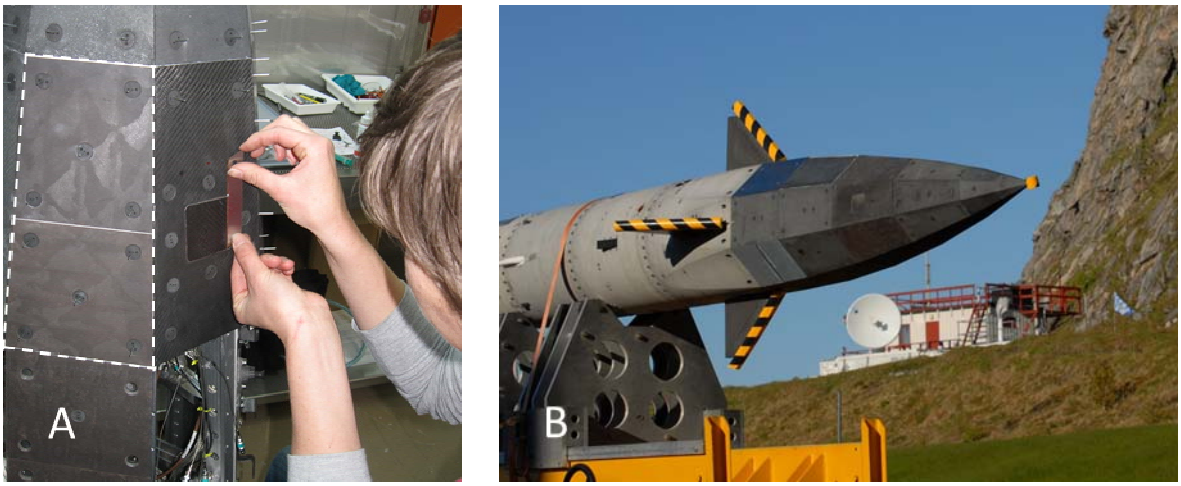

Fig. 1. Integration of the WHIPOX panels (A) as part of the thermal protection system of the SHEFEX II reentry vehicle (B). The vehicle was successfully launched in June 2012.

The microstructure of WHIPOX is shown in Figure 3 below. The composite material consists of oxide fibers (commercial Nextel fibers of type 610, 650 and 720) which are embedded in a porous matrix of alumina or alumina rich aluminosilicates [3-5]. In an ideal situation the fiber distribution within the porous matrix is homogeneous. However, the winding process during fabrication induces some uneven fiber filament arrangements and matrix agglomerations. Depending to the winding angle and the thickness of the laminate, the effect of fiber displacement becomes more or less significant.

Fig. 2. Two uncoated WHIPOX components of the SHEFEX II TPS

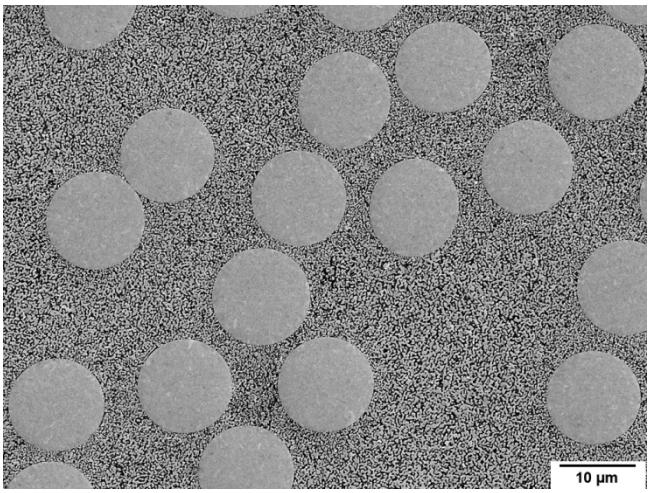

Fig. 3. SEM image of the WHIPOX microstructure with typical microporosity within the alumina rich matrix

1. Manufacturing Process

The manufacturing of WHIPOX CMCs is based on slurry infiltration of the fiber bundles and a subsequent winding process. First of all the coating of the fiber bundles is removed, followed by the infiltration process in aqueous slurry. Thereafter, the infiltrated fiber rovings are wound up on suitable mandrels by using computer controlled winding systems which are capable to adjust a broad range of fiber orientations (Fig. 4). After the winding process is completed, the flexible green body is cut lengthwise and removed from the mandrel. After flattening or shaping the material, it is dried and sintered at temperatures around 1300 °C (Fig. 5). Although the green body is quite flexible in the moist state, the

flattening and the forming of the laminate may lead to displacements of the filament bundles and therefore microstructural inhomogeneity. Moreover, the fiber cross-over points which are a typical feature of the winding process are creating local zones of increased porosity. The intermediate pore size of these zones and the periodic shift of the crossing points across the laminate's thickness are strongly influenced by the winding angle and the thickness of the fiber rovings [4,5].

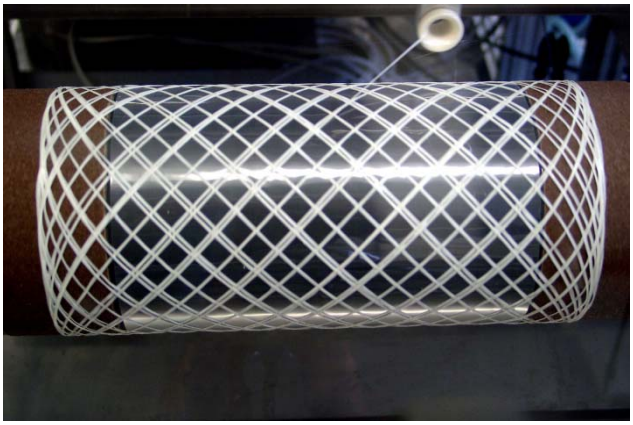

Fig. 4. Arrangement of oxide fiber rovings during the winding process

Fig. 5. WHIPOX plate in its final condition after flattening and sintering (original surface)

Until now, the influence of winding patterns and shaping processes on resulting microstructural defects is still not well understood. The microscopic defects analyzed so far are matrix agglomerations with shrinkage pores, large pores of the fiber's cross-over points and local delamination. The influence of such defects on the material's mechanical properties is still under investigation. Generally, the characterization of production-related flaws in WHIPOX CMCs is challenging because the definition of objective features for distinguishing between inherent matrix porosity (Fig. 3) and "true" defects caused by the variance of processing parameters is quite difficult. Thus, non-destructive inspection techniques are indispensable methods for monitoring and categorizing microstructural features and flaws within the composite material.

2. Non-destructive Characterization

2.1 Overview

Table 1 shows all investigations that have been performed for this work with the three different WHIPOX sample plates W1233, W1262 and W1289.

Table 1. Sample overview and performed investigations

Sample plate	**W1233**	**W1262**	**W1289**
Fiber orientation	± 45°	± 45°	± 45°
Thickness	3 mm	5 mm	10 mm
NDT inspection	- Air coupled ultrasound - Lock-in thermography - 3D Terahertz - Computed tomography	- Air coupled ultrasound - Lock-in thermography - Computed tomography	- Air coupled ultrasound - Lock-in thermography - 3D Terahertz - Computed tomography
Mechanical testing	--	- Tensile test - Shear test	--

2.1 Air-coupled Ultrasound Inspection

All three plates were inspected by using air-coupled ultrasound (ACU). The C-mode image of plate W1233 shown in Figure 6 was obtained with a through transmission mode technique. The transducer's frequency was about 180 kHz. As the dashed lines indicate, the rhombic fiber bundle structure is slightly visible in the ultrasound image. As the very view dark blue tinted areas confirm, there are no significant defects in this WHIPOX plate. For comparison, Figure 7 shows a photographic image of a part of the plate's surface structure.

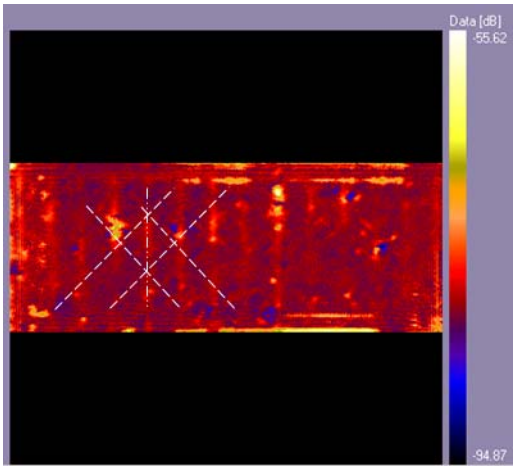

Fig. 6. Air-coupled ultrasound scan of plate W1233 (C-mode)

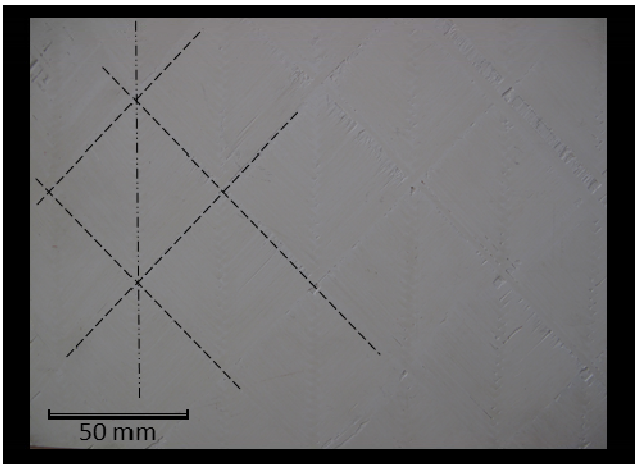

Fig. 7. Photographic view of a surface segment of WHIPOX plate W1233 (grinded surface)

Figure 8 shows an ultrasound image of WHIPOX plate W1289 which is rather thick (approx. 10 mm). The dark blue tinted areas in this scan indicate that there is high ultrasound signal attenuation in these areas. Locally increased porosity or delamination is the most likely explanation for this phenomenon. However, the blue areas are localized along horizontal lines. Regarding the number of lines as well as the distances observed in the C-mode ultrasound scan, it seems that the defective blue areas are in good correlation with the interspaces of the horizontal lines that are visible on the material's surface (cf. Fig. 9). These lines on the photographic image are showing the so called cross-over points of the wound fiber rovings (cf. Fig. 4 & 5). Thus, the defects found by ultrasound inspection are obviously located in between these rows of cross-over points.

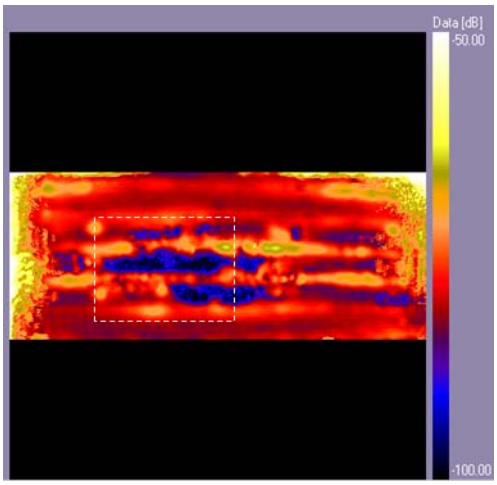

Fig. 8. Air-coupled ultrasound scan of plate W1289 (C-mode)

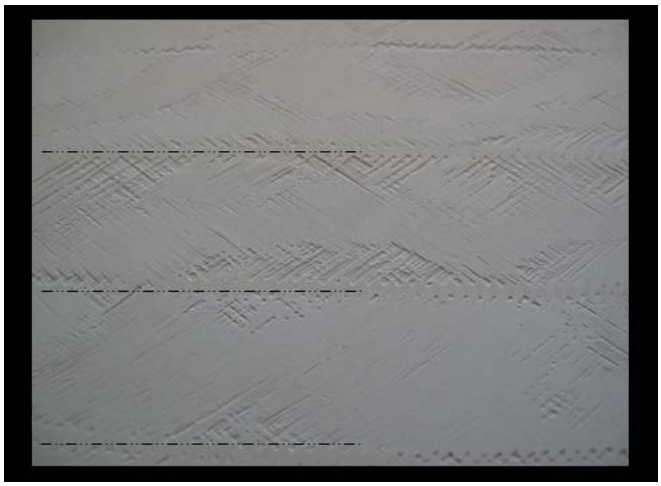

Fig. 9. Photographic view of a surface segment of WHIPOX plate W1289 (grinded surface)

2.2 Optically Excited Lock-in Thermography

Figure 10 and 11 are showing phase images of optically excited lock-in thermography (OLT) inspections from parts of plate W1233. The lower the excitation frequency *f*, the higher is the thermal diffusion length μ [6]. As a consequence, the phase image of Figure 10 shows more surface features than that of Figure 11. The penetration depth of the thermal waves in WHIPOX material is approximately 14 mm for f = 0.06 Hz and 34 mm for f = 0.01 Hz. Thus, in the phase images there is also information included which is from thermal waves reflected by the plate's back side (see Table 1). The rhombic fiber filament structure is clearly identifiable in both OLT images and the vertical lines are marking cross-over points of the filament bundles (cf. Fig. 6). In this plate there are no details visible that could be identified as signals from significant material flaws.

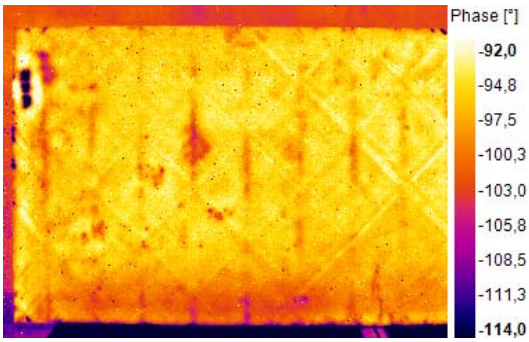

Fig. 10. Phase image of plate W1233 (f = 0.06 Hz)

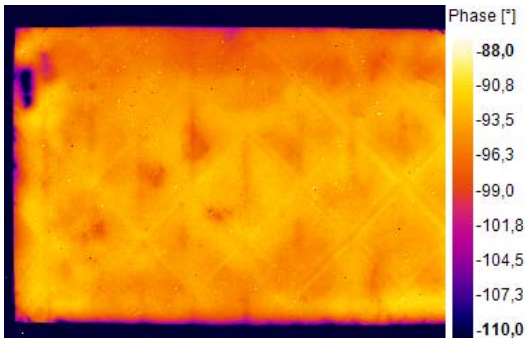

Fig. 11. Phase image of plate W1233 (f = 0.01 Hz)

Figure 12 shows the OLT phase image of plate W1262 at f = 0.01 Hz. This plate is 5 mm thick and shows the rhombic structure as well. Here the material is interspersed with defects which are indicated by the dark blue and purple tinted areas. The corresponding ultrasound scan is shown on the right (Fig. 13). The locations of material defects are obviously aligned in horizontal and vertical orientation which is certainly connected with the rhombic fiber filament structure and the resulting cross-over points. Local areas of delaminated material or aggregations of porosity are the most likely interpretation.

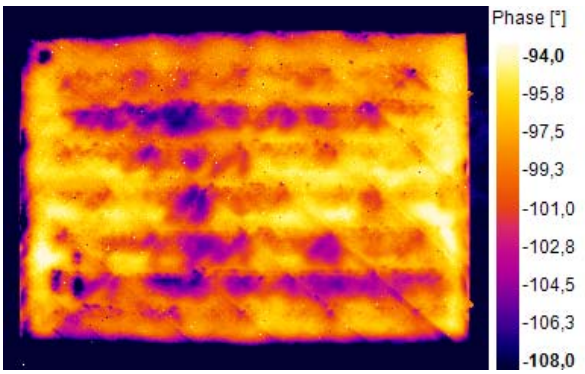

Fig. 12. Phase image of plate W1262 (f = 0.01 Hz)

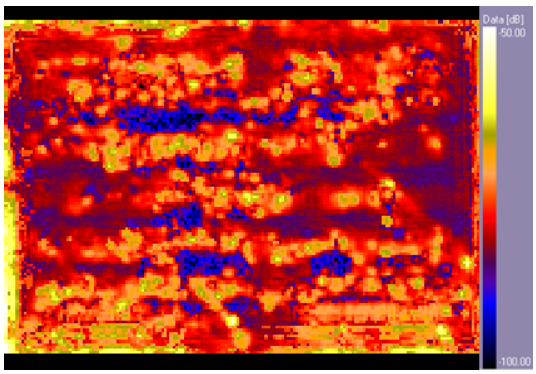

Fig. 13. Corresponding ACU scan of plate W1262

Although the matrix of WHIPOX is always interspersed with numerous microscopic pores, the defects found here have nothing to do with that kind of inherent microporosity that is shown in Figure 3. Pores of that size are by far too small to be detected with OLT or ultrasound techniques. Nevertheless, the focus of this kind of inspections is set to larger process-related defects in the range of 10 – 10^4 µm which may deteriorate the mechanical properties of the CMC material. It turned out that with increasing laminate thickness the probability of detecting such defects is increasing as well.

2.3 Terahertz Inspection

It is the very first time that the WHIPOX material is inspected with terahertz technology (THZ). The details about the measurement conditions are reported by Becker [7]. Figure 14 shows the total reflection signal image mapping of the surface region from plate W1233. It is the corresponding image to the ultrasound C-scan shown in Figure 6 and the OLT phase image in Figure 10. At the first sight the filament's rhombic structure comes out very clear. There are no single fibers visible but the gaps and interspaces along the lines of roving structures. The locations of the cross-over points of the oxide fibers are clearly detectable as they are aligned in vertical rows. However, this is changing fundamentally as soon as the focused XY-layer is located beneath the plate's surface region [7]. With deeper penetration along the Z-axis only surfaces and boundaries of increased reflectivity within this layer are visible while the filament structures are not directly visible anymore. On the other hand single defects within the focused XY-layer are coming out very clear.

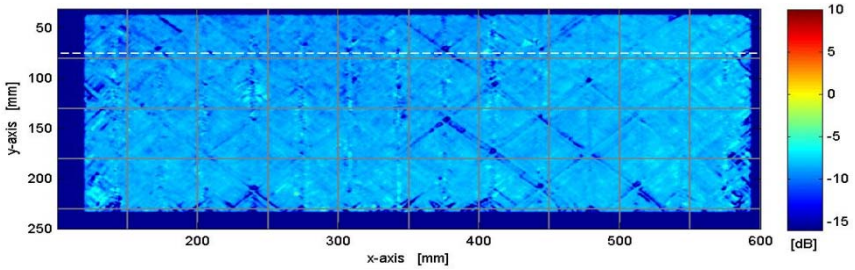

Fig. 14. C-scan image of WHIPOX plate W1233 at 0.3 THz

Figure 15a shows a C-scan image of the inside structure of plate W1289. The Z-position is located approximately 2.5 mm below the plate's surface. The reflectivity image scan reveals some defect signals at certain positions. Judging from the size, location and extension, the signals are quite similar to that of the corresponding ultrasound image (cf. Fig. 8). The dashed horizontal line in Figure 15a goes right through and marks the location of the B-scan image on the right (Fig. 15b). The B-scan is like a cross-section through the plate's thickness (XZ-plane). Beside the plate's front and back side surface echoes, it shows the depth locations of any defect in this plane. The defect's signal addressed here is located approximately 2-3 mm underneath the material's surface. By contrast to the lock-in thermography imaging, the location in depth can be displayed in a B-scan mode.

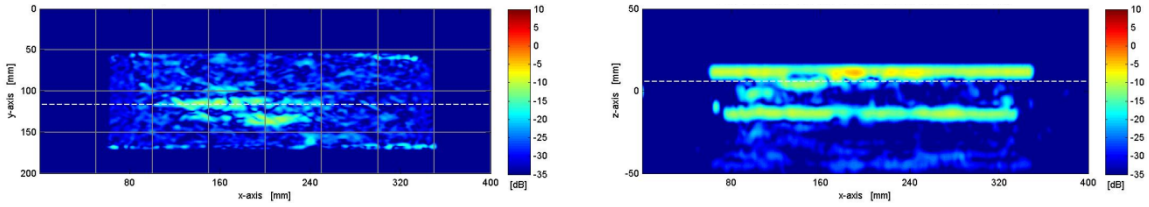

a) b)

Fig. 15. a) C-scan of WHIPOX plate W1289 at 0.1 THz. b) the B-scan is representing a cross-section view with a front and a back side surface echoe of the plate

2.4 Computed Tomography

The three CMC plates W1233, W1262 and W1289 were also investigated with X-ray based computed tomography (CT). Strictly speaking, only regions of special interest (ROI) were inspected with µ-CT at voxel sizes around 28-42 µm and with nano-CT at 4.5 µm (see chapter 3). While Figure 16 shows a schematic illustration of several fiber rovings in a

cross-over region, the real microstructure of such a section is depicted in Figure 17, viewing along Y-axis (left image) and along X-axis (right image). The microstructure is a small ROI of plate W1233 (voxel size: 28.2 µm). Beside the cross-over structure of the filament bundles, there are also a view very small cracks and shrinkage pores visible which are all part of the matrix (Fig. 17, left image).

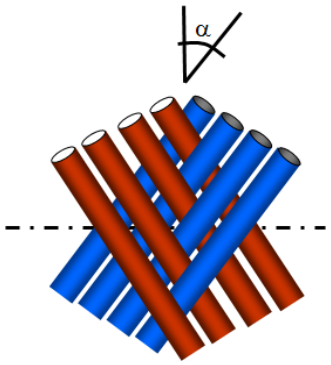

Fig. 16. Schematic illustration of a fiber roving cross-section

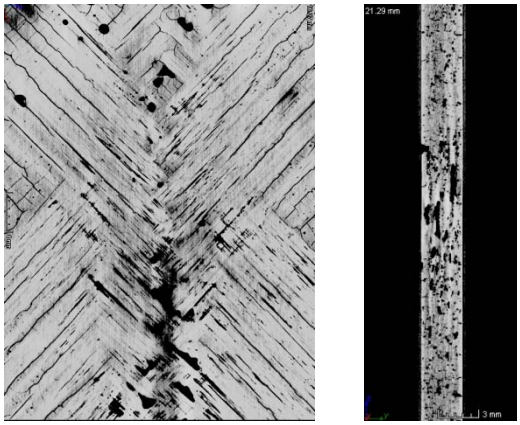

Fig. 17. CT-images of a fiber roving cross-section in plate W1233 (voxel size: 28.2 µm)

Figure 18 to 20 show CT images of a ROI scan of plate W1289 (voxel size: 42.2 µm). A typical filament displacement is depicted in Figure 18. The distribution of these kind of defects is statistical and can be found almost everywhere in the WHIPOX microstructure. However, Figure 19 shows a local delamination which is outlined with an arrow in the cross-section views beside (Fig. 20). It is exactly the delaminated area which caused the defect signal in the Terahertz scan (Fig. 15a & 15b) and the ultrasound scan (Fig. 8) and was located in a depth about 2-3 mm beneath the material's surface. Furthermore, the upper two cross-section views (Fig. 20) both show the horizontal shift of small pores across the laminate's thickness. These are the gaps which are caused by the cross-over fiber regions.

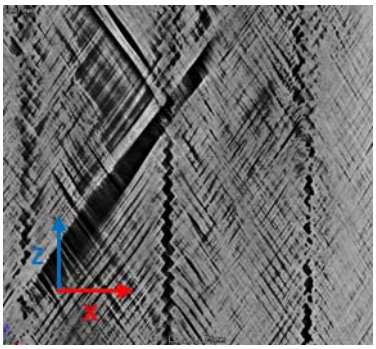

Fig. 18. Filament displacement in plate W1289 (CT image)

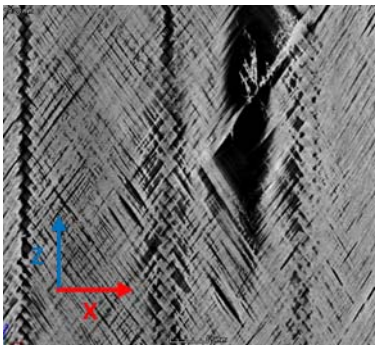

Fig. 19. Delamination in plate W1289 (CT image)

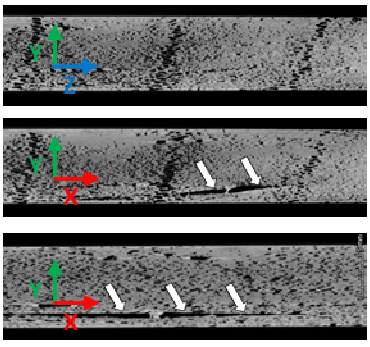

Fig. 20. Cross-section views of delaminated areas (CT images)

2.5 Evaluation

The non-destructive investigation techniques used so far to analyze the microstructure of the WHIPOX CMC material have shown that the process-relevant defects can be detected with more than just one method. Some of them are capable to inspect wide-spread areas of a large panel or structure component with relatively low resolution while other methods are

predestined for high resolution inspection on ROI which are sometimes not larger than a few square millimeters. Some of them are good for detecting defects at all while others are showing the exact location (e.g. in depth) or microscopic dimensions of the defects. However, Table 2 resumes the experience with WHIPOX inspection made so far.

Table 2. Detectability of microstructural details and flaws in WHIPOX CMC

	ACU	OLT	THZ	CT
Fiber alignment	–	(+)[a]	(+)[a]	+[b]
Fiber rovings	–	(+)[a]	(+)[a]	+
Fiber cross-over points	(+)[a]	(+)[a]	(+)[a]	+
Gap width between fibers/fiber rovings	–	–	(+)[a]	+[b]
Porosity aggregation (between fibers/layers)	+	+	+	+[b]
Single pores (size, morphology, orientation)	–	–	–	+[b]
Microcracks (translaminar)	–	(+)[d]	–	+[b]
Microporosity (matrix)	–	–	–	–
Fiber/matrix volume fraction	–	–	–	+[c]
Layered microstructure	–	(+)[a,d]	–	+[b]
Stacking sequence	–	–	–	+[b]
Foreign inclusions	+[d]	+[d]	+[d]	+[b,d]
Delamination (laminary extension)	+	+	+	(+)[b,d]
Delamination (perpendicular extension)	–	–	–	(+)[b]
Delamination location (depth)	(+)[a,c]	+	+	+

[a)] depending to measurement parameters & CMC type
[b)] depending to detail resolution
[c)] depending to evaluation software
[d)] depending to feature's size & orientation

3. Mechanical Properties and Non-destructive Material Characterization

In order to determine differing mechanical properties of samples from one single oxide CMC plate, the OLT phase image of plate W1262 was used as a reference for porosity distribution (cf. Fig. 12, 21a). As previously reported, there are several regions of different porosity that were clearly identified within the plate. The mechanical properties were determined from tensile and shear tests. Regarding the load direction of the test samples, the fiber orientation was ±45° (Fig. 21b, 21c). The tensile test samples measured 150 mm in length with a waist line cross-section of 8 x 5 mm² and 50 mm in length (Fig 21b). The Iosipescu shear samples were notched on both sides with the angle of 110° (Fig 21c).

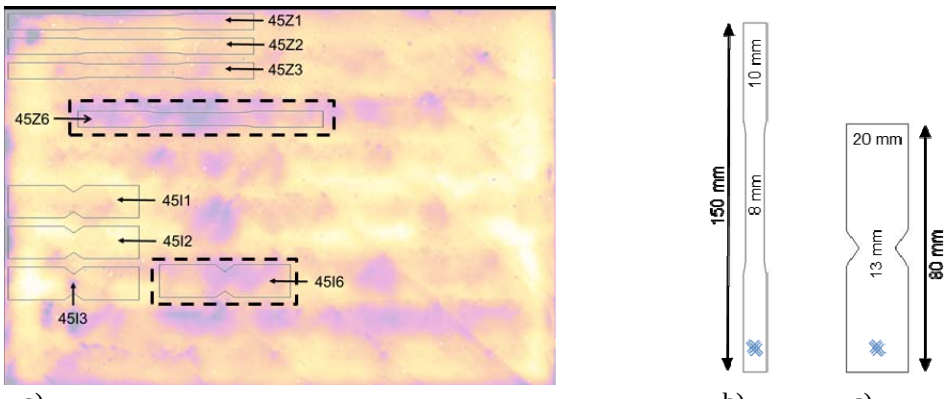

a) b) c)

Fig. 21. a) Correlation of OLT image information and test specimen selection for tensile and Iosipescu shear testing. Specimens 45Z6 and 45I6 were prepared from areas of increased porosity (outlined by dark purple color); b) tensile test sample dimensions (150 x 10(8) x 5 mm³) and fiber orientation (±45°); c) Iosipescu shear test sample dimensions (80 x 20(13) x 5 mm³) and fiber orientation (±45°)

All mechanical tests were performed at room temperature under quasi-static load and the specimens were tested in a spindle driven device. The strain was measured with strain gauges in longitudinal as well as transverse direction for tensile tests and in ±45° direction for shear tests. The main objective is the verification of correlations between the material's local porosity and its mechanical properties. Thus, the microstructure of two different tensile specimens (45Z2 and 45Z6) and two different Iosipescu shear specimens (45I2 and 45I6) were analyzed with high resolution CT inspection. Strictly speaking, it is a very small cube shaped volume (cube's edge size: 3.6 mm²) from the specimen's estimated failure zone that was analyzed with CT. The minimum voxel size of these CT-scans was 4.5 µm. Hence, structural details of >10 µm were principally detectable under these conditions. Figure 22 below shows the reconstructed 3-dimensional volumes of specimen 45Z6 and 45I6 which were both cut out from areas with increased porosity (cf. Fig. 21).

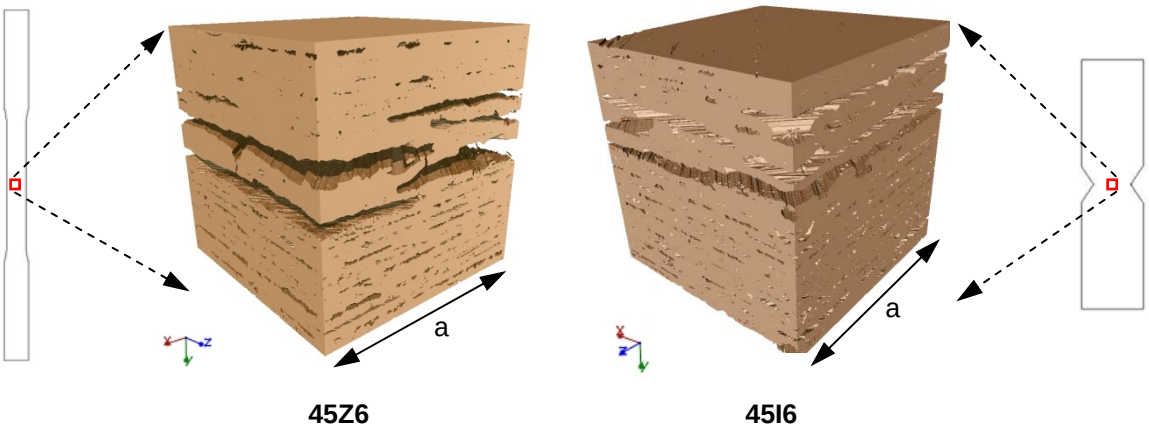

Fig. 22. CT based analysis of local porosity distribution in the center area of tensile test specimen 45Z6 and shear test specimen 45I6 (a = 3.6 mm)

While the brown phase of these images depicts the 3-dimensional distribution of oxide fibers with the surrounding oxide matrix, the interlaminar pores and gaps between the fiber bundles are visible as elongated, almost even tubular-like cavities in between the laminate microstructure. Of course, the geometry of these cavities is strongly influenced by the oxide fiber's orientation. As the two 3-dimensional CT images indicate for both samples, there is a cumulation of larger pores in some layers of the CMC's laminate. These are the defects that were detected with OLT and ultrasound inspection (compare to Fig. 12 & 13, 21).

As shown in Figure 23, there is considerable different mechanical behavior between the specimens from porous locations (45Z6 & 45I6) and those of other locations with more dense material (45Z1-3 & 45I1-3). In the case of sample 45Z6, the material fails already at a relatively low stress level of 70 MPa which is approximately only 70% compared to the load levels of the other samples (Fig. 23a). Regarding the shear test samples, the porous material (45I6) also shows a relatively low strength and shear modulus compared to the other samples (45I1-3) (Fig. 23b). It should be noted that some strain gauges broke earlier than the shear samples (45I2 & 45I3). However, it is obvious that there is a correlation between the detected porosity and the mechanical properties of the test specimens.

According to the data that is shown in Table 3 below, sample 45Z6 with relatively high local porosity e´ shows lower tensile strength and Young's modulus than the sample 45Z2. The local porosity e´ was determined from CT-based measurements. It is representative for a small cube-shaped volume element of approximately 47.7 mm³ that was extracted from the center area of the specimen (see Fig. 22). The same goes for the shear test specimens.

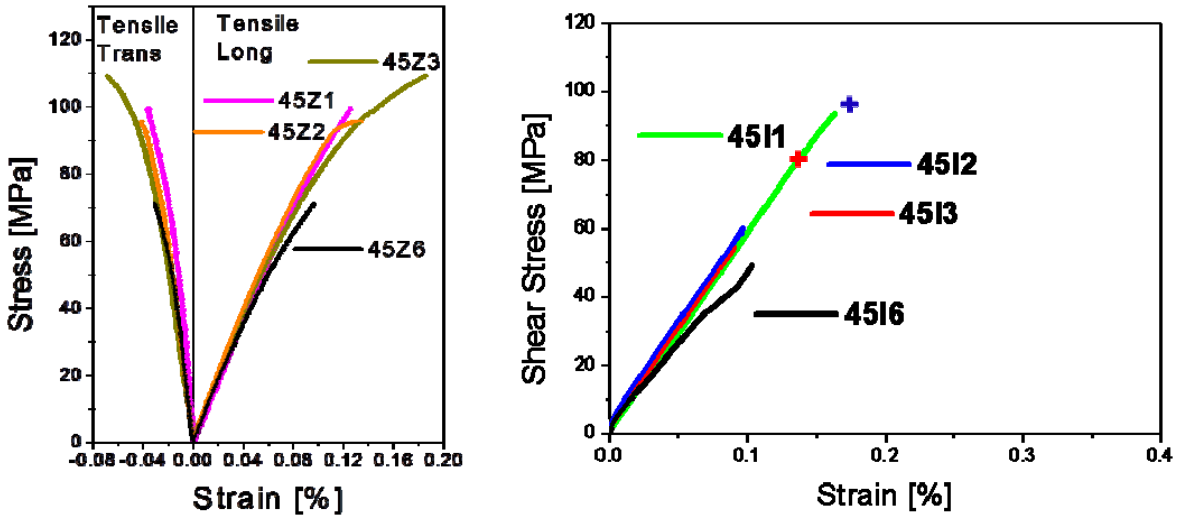

a) b)

Fig. 23. Stress-strain curves of WHIPOX composite: a) tensile testing with longitudinal and transverse strain gauges; b) Iosipescu shear testing with strain gauges in ±45° orientation

Table 3. Sample overview and performed investigations

Specimen		Porosity e´	Strength σ	Modulus E/G
		[%]	[MPa]	[GPa]
Tensile test	45Z2	17.00	95.73	100.37
	45Z6	20.50	71.32	93.09
Shear test	45I2	9.40	102.79	59.84
	45I6	19.70	53.96	49.60

4. Conclusions

Establishing an effective quality assurance system is not only a question of using a bunch of non-destructive test methods in a processing route but to achieve fundamental knowledge about the decisive manufacturing steps, tolerances, deviations and the relevance of defects that may occur. Choosing and developing the right inspection techniques is just one aspect of many others in the wide field of process-integrated quality assurance management. However, it is important to find inspection methods that are capable to provide all the information that is needed to understand and to control every single manufacturing step. The methods that are shown in this work may be categorized in two main groups: those that allow a fast analysis which covers a wide-spread area of CMC panel or a large structure component with less resolution and others that enable high precision analysis of a small material volume. Certainly, computed tomography provides more detailed information about a composite's microstructure than any other inspection technique and is therefore an excellent reference method for enhanced signal interpretation. But focusing the smallest details also means that the detectable sample volume becomes quite small as it is shown with the nano-CT inspection on the mechanical test specimens. Thus, the view turns more and more into a material characterization in which the context between structural aspects (e.g. roving cross-over zones, fiber orientation) and observed defect patterns are gradually lost from sight. In terms of a consistently process monitoring and effective quality assurance other strategies are needed. In contrast, inspection

techniques like contactless air-coupled ultrasound, optically excited lock-in thermography or even the new terahertz imaging technology turned out to be quite good for reliable overview measurements on WHIPOX material. The examples shown here have proven that these methods are even more suitable for inspections on larger structure components since they can be operated within a minimum of measurement time and by far less technical effort than with CT.

References

[1] J. Göring, S. Hackemann, B. Kanka: *"WHIPOX®: A fiber-reinforced oxide-ceramic matrix composite for long-term high-temperature applications"* (in German), Mat.-wiss. U. Werkstofftech., 38, No. 9 (2007), p. 766-772.

[2] H. Böhrk, H. Elsäßer, H. Weihs: *"The SHEFEX II Thermal Protection System"*, Proc. 7th Symp. on Aerothermodynamics for Space Vehicles, on CD (2011); http://elib.dlr.de/71039/

[3] M. Schmücker, A. Grafmüller, H. Schneider: *"Mesostructure of WHIPOX all oxide CMCs"*, Composites: Part A, 34 (2003), p. 613-622.

[4] B. Kanka, M. Schmücker, W. Luxem, H. Schneider: *„Processing and Microstructure of WHIPOX™"* – published in: High Temperature Ceramic Matrix Composites (Ed.: W. Krenkel, R. Naslain and H. Schneider), Wiley-VCH, Weinheim (2001), p. 610-615.

[5] M. Schmücker, P. Mechnich: *"All-Oxide Ceramic Matrix Composites with Porous Matrices in Ceramic Matrix Composites"* – published in: Fiber Reinforced Ceramics and their Applications (Ed.: W. Krenkel), Wiley-VCH, Weinheim (2008), p. 205-229.

[6] T. Ullmann, Y. Shi, R. Aoki: *"Capabilities of Lock-in Thermography for Non-destructive Inspection of Fibre Reinforced Composites"*, Proc. 11th Int. Conf. on Quantitative InfraRed Thermography – QIRT (2012), published online: http://www.ndt.net/article/qirt2012/papers/QIRT-2012-384.pdf

[7] S. Becker, T. Ullmann, G. Busse: *"3D Terahertz Imaging of Hidden Defects in Oxide Fibre Reinforced Ceramic Composites"*, to be published on Proc. 3rd Int. Symp. for NDT in Aerospace (2012)